RSC Advances

ROYAL SOCIETY OF CHEMISTRY

www.rsc.org/advances

Oxygen-loss in A-site deficient $Sr_{0.85}La_{0.10}TiO_3$ perovskite

Ipek Akin[1], Ming Li[2], Zhilun Lu[2], Derek C. Sinclair[2,*]

[1]Department of Metallurgical and Materials Engineering, Istanbul Technical University, Istanbul, 34469, Turkey

[2]Department of Materials Science & Engineering, University of Sheffield, Sheffield, S1 3JD, UK

*Corresponding Author's e-mail: d.c.sinclair@sheffield.ac.uk

Abstract

The electrical properties of $Sr_{1-3x}La_{2x}TiO_3$ ceramics (x=0.05, LST) change dramatically with sintering temperature and atmosphere. Ceramics sintered at 1200 ℃ in both O_2 and N_2 exhibit near intrinsic band-type conduction with bulk conductivity ~ 10^{-7} Scm^{-1} at 500 ℃ and activation energy for conduction, E_a of ~ 1.6 - 1.8 eV. LST ceramics sintered at 1450 ℃ in O_2 exhibit much higher bulk conductivity (> 10^{-4} Scm^{-1} at -50 ℃) with an E_a ~ 0.16 eV. For LST ceramics sintered at 1450 ℃ in N_2, the bulk conductivity was too high to be measured by Impedance Spectroscopy even at 10 K. In addition, electrical heterogeneity is observed in LST pellets sintered at 1450 ℃ under both O_2 and N_2 where pellet outer surfaces are more resistive than the inner regions of the ceramic. The defect chemistry of $Sr_{0.85}La_{0.10}TiO_3$ perovskite is discussed based on chemical doping and oxygen-loss mechanisms and we highlight the importance of A-site vacancies on the oxygen-loss mechanism in La-doped ST-based ceramics.

Table of contents entry

Sintering temperature induces significant changes in bulk conductivity and activation energy, E_a of A-site deficient $Sr_{0.85}La_{0.10}TiO_3$ due to oxygen loss.

Graphical Abstract

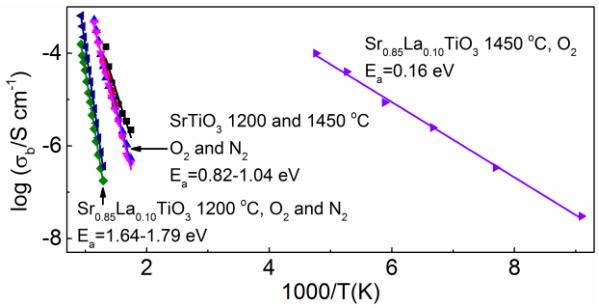

Introduction.

Chemically doped (Ba,Sr)TiO_3-based ceramics exhibit a wide variety of electrical properties spanning dielectric behaviour[1], mixed oxide-ion/electronic conduction[2] and superconductivity.[3,4] In particular, the dielectric materials are utilised in multilayer ceramic capacitors, Pb-free piezoelectrics and non ohmic (positive temperature coefficient resistor, ptcr) thermistors whereas there has been much recent interest in reduced rare earth doped $SrTiO_3$ materials as anodes for solid oxide fuel cells (SOFCs).[5] For many years it has been unclear whether A- or B-site vacancies are the main compensating point defects in La-doped (Ba,Sr)TiO_3-based perovskites, at least for those prepared in air and why many of these materials often exhibit appreciable levels of electronic conduction.[5-15]

La is unique amongst the trivalent rare earth (RE) ions as it is sufficiently large that it substitutes exclusively on the A-site of (Ba,Sr)TiO_3; intermediate sized RE ions such as Gd can self-compensate by substituting on the A- and B-site in equal amounts to avoid the creation of cation vacancies; small RE ions such as Yb substitute exclusively on the B-site with the creation of oxygen vacancies. Equilibrium ternary phase diagram studies conducted in air show clear evidence of B-site vacancies for La-doping in $BaTiO_3$, based on a general formula $Ba_{1-x}La_xTi_{1-x/4}O_3$ with $0 \leq x \leq 0.20$ at 1350 ^oC.[13,15,16] Such materials should exhibit dielectric behaviour for all values of x; however, it is well known that processing in air, especially for low levels of A-site doping can result in semiconducting and functionally graded ceramics, some of which are used as the basis for ptcr thermistors.[17] This led to the popular belief that electronic compensation by donor-doping based on a general formula $Ba_{1-x}La_xTi^{4+}_{1-x}Ti^{3+}_xO_3$ may exist, especially for low levels of x.[14] Acceptance of this mechanism grew after atomistic simulations suggested electronic donor-doping to be the most favourable defect mechanism,[18] despite the absence of any measurable solid solution in the ternary phase diagram. In previous studies, we have used Impedance Spectroscopy (IS) to probe the electrical microstructure of single-phase $Ba_{1-x}La_xTi_{1-x/4}O_3$ ceramics sintered at 1350 ℃ in air, O_2 and Ar.[15,17,19,20] Samples processed in O_2 were excellent dielectrics across the entire solid solution and exhibited electrically homogeneous microstructures consisting of insulating grain and grain boundary regions. Such results are consistent with the equilibrium phase diagram studies.[13,16]

Samples processed in air and Ar showed electrically heterogeneous microstructures consisting of a combination of semiconducting grains, core/shell grain phenomena, insulating grain boundaries, and resistive surface layers, depending on a combination of processing parameters.[15,19] The processing parameters include; the doping level (x); pO_2; sintering temperature and time; and the heating and cooling profiles during sintering. All of these can influence the ceramic microstructure and therefore the level and distribution of oxygen-loss on heating and the re-oxidation on cooling. This demonstrated the influence of kinetics on the observed electrical properties and led us to suggest the source of semiconductivity in La-doped $BaTiO_3$ ceramics processed in air or an inert atmosphere such as N_2 and Ar at 1350 ℃ is associated with oxygen loss from the lattice from the well-known mechanism based on Kroger-Vink notation

$$O_O^x \rightarrow V_O^{\bullet\bullet} + \tfrac{1}{2} O_2\,(g) + 2\,e^{/} \quad \text{(equation 1)}$$

The production of electrons by this process can induce semiconductivity by partial reduction of Ti^{4+} to Ti^{3+} ions and resolve the discrepancies between the equilibrium phase diagram studies and measured electrical properties. If samples are not processed in O_2 to suppress this oxygen-loss mechanism which can occur at the common sintering temperature of 1350 ℃ for $BaTiO_3$-based ceramics, homogeneous dielectrics cannot be obtained and the ceramics are electrically heterogeneous and based on a general formula of $Ba_{1-x}La_xTi_{1-x/4}O_{3-\delta}$ where δ represents net oxygen-loss during ceramic processing.

Recently, an improved set of potentials has been developed for $BaTiO_3$ and atomistic simulations for RE dopants have shown the electronic donor doping mechanism to be highly unfavourable, irrespective of the size of the RE dopant.[21] Furthermore, calculations for La-doping showed the creation of B-site vacancies with subsequent oxygen-loss to give a general formula $Ba_{1-x}La_xTi_{1-x/4}O_{3-\delta}$ that was a factor of two more favourable than electronic donor-doping based on the general formula $Ba_{1-x}La_xTi^{4+}_{1-x}Ti^{3+}_xO_3$.[22] These results verified our earlier suggestions that the source of semiconductivity and electrical heterogeneity in La-doped $BaTiO_3$ ceramics processed in air is associated with oxygen-loss at elevated temperatures combined with partial re-oxidation on cooling of the ceramics. It would appear the presence of B-site vacancies play an important role in facilitating the oxygen-loss mechanism in La-doped $BaTiO_3$ ceramics.

Several groups have shown experimental evidence for an extensive solid solution between $SrTiO_3$ and $La_{2/3}TiO_3$ for samples prepared in air, suggesting the existence of A-site vacancies in this system.[6-9,23] Based on a general formula of $Sr_{1-3x/2}La_xTiO_3$ Howard et al[23] have suggested a random distribution of A-site vacancies for x = 0.20 based on a cubic ($Pm\bar{3}m$) unit cell at room temperature (RT), whereas cation ordering becomes increasing prominent at higher x with a lowering of the RT crystal symmetry to tetragonal (I4/mcm) at x~ 0.30 and finally to orthorhombic at RT at $x \geq 0.55$. The existence of A-site vacancies in La-doped $SrTiO_3$ as opposed to B-site vacancies or electronic donor-doping has recently been suggested by Dawson et al[24] based on atomistic simulations. Similar to the case for $BaTiO_3$, electronic donor-doping of La on the A-site was deemed to be energetically unfeasible in $SrTiO_3$ compared to the formation of metal vacancies, at least for samples prepared in air.

$SrTiO_3$-based compounds have been widely investigated as viable anodes for SOFCs [2,5,25-27] as they can exhibit metallic conduction when exposed to reducing conditions and high temperatures due to reduction of Ti with creation of oxygen vacancies, as given in equation (1). Interestingly, Irvine et al have shown that A-site deficient $La_xSr_{1-3x/2}TiO_3$ compositions exhibit higher conductivity than stoichiometric (donor-doping) compositions, $La_xSr_{1-x}TiO_3$ at the same oxygen partial pressure.[26,27] Furthermore, processing in 5 % H_2 at 1400 ℃ can result in very high electronic conductivity, eg 80-400 Scm^{-1} at 800 ^oC at $pO_2 = 10^{-14}$ Pa (typical SOFC conditions) presumably due to stripping of oxygen from the lattice.[28]

Here we report the influence of A-site vacancies in $La_{0.10}Sr_{0.85}TiO_3$ (LST) on the oxygen-loss model that has been observed for B-site deficient $La_{1-x}Ba_xTi_{1-x/4}O_3$ by processing LST ceramics at 1200 and 1450 ℃ in flowing O_2 and N_2 and assessing their electrical microstructures via IS. This leads to a better understanding of the conditions required to obtain homogeneous and heterogeneous dielectrics based on La-doped $SrTiO_3$.

Experimental.

Samples of $SrTiO_3$ (ST) and $Sr_{1-3x}La_{2x}TiO_3$ with x=0.05 (LST) were prepared by the conventional solid state, mixed oxide route. Appropriate amounts of pre-dried $SrCO_3$ (Aldrich, 99.98%), La_2O_3 (Aldrich, 99.99%) and TiO_2 (Aldrich, +99.9%) powders

were ball milled for 8 h in isopropanol using a polyethylene bottle and yttria stabilized zirconia milling media. The mixed powders were placed in a platinum crucible and calcined at 1050 ℃ for 6 h. The powders were ball milled for 8 h, sieved and reacted at 1250 ℃ for 10 h in air. Pellets were prepared by uniaxial pressing of reacted powders at 40 MPa in an 8 mm die followed by pressing at 200 MPa in a cold isostatic press. The green bodies were placed in an alumina boat lined with Pt foil and sintered in a tube furnace at 1200 or 1450 ℃ for 6 h in flowing O_2 or N_2 with a heating and cooling rate of 5 ℃/min.

Ceramic density was determined by measuring pellet mass and dimensions for samples sintered at 1200 ℃ and by the Archimedes method for samples sintered at 1450 ℃. Relative density was calculated as a percentage by comparing the physical density with the theoretical X-ray density.

X-ray Diffraction (XRD) was performed using a high-resolution STOE STADI-P diffractometer (STOE & Cie GmbH, Darmstadt, Germany) with a linear position sensitive detector (PSD), Cu $K\alpha_1$ radiation. Data were collected over the 2θ range of 20-100 °with Si as an internal standard. Lattice parameters were calculated using a commercial software package, WinXPow.

Ceramic microstructure was examined using an FEI Inspect F Scanning Electron Microscope (SEM). Cross sections of representative samples sintered at 1450 ℃ were polished and thermally etched. For samples sintered at 1200 ℃, fresh fracture surfaces were examined. All samples were carbon-coated.

Impedance spectroscopy (IS) data were collected on electroded ceramics over the frequency range 10 to 10^7 Hz using a Hewlett-Packard 4192A instrument with an applied voltage of 100 mV. Electrodes for IS measurements of all ceramics sintered at 1200 ℃ and for ST ceramics sintered at 1450 ℃ were prepared from an organogold paste (Engelhard T-10112). The electroded pellets were fired at 800 ℃ for 2 h to remove organics and harden the Au residue. IS was performed from 300 to 800 ℃ in various atmospheres, including O_2 and N_2 gas to establish the oxygen partial pressure dependence of the bulk (grain) conductivity. LST ceramics sintered at 1450 ℃ were electroded by either spreading InGa (40/60 mol %) alloy or sputtering Au onto the freshly ground faces. An Emitech K575D dual head sputter coater with a sputtering

current of 30 mA and a sputtering time of 5 min was used to fabricate the sputtered Au electrodes. IS data were collected as appropriate, either at elevated temperatures (~ 250 – 800 ℃) using a home-made jig and a non-inductively wound tube furnace or by an Oxford Instruments cryocooler system (10 – 300 K). All IS data were corrected for sample geometry.

Results.

X-ray diffraction analysis showed all ceramics to be single phase, irrespective of the sintering temperature and atmosphere. All were indexed on a cubic unit cell (space group $Pm\bar{3}m$). There is no obvious change of lattice parameter values with sintering conditions for both ST samples (3.90540(6)-3.90557(19) Å) and LST samples (3.90104(9)-3.90233(12) Å), Table 1. Pellet densities were ~ 61-70 and ~ 97-99 % for ceramics sintered at 1200 and 1450 ^{o}C for 6 h, respectively, Table 1. The grain size of ceramics sintered at 1450 ^{o}C was ~ 10-20 and ~ 5-10 μm for ST and LST, respectively, Fig S1. Ceramics sintered at 1200 ℃ exhibit smaller grain size ~1-2 μm, Fig S1.

Impedance complex plane, Z*, plots for ST ceramics in the range ~ 250-550 ℃ consist of two overlapping arcs and could be modelled on an equivalent circuit based on two parallel RC elements connected in series. R values were extracted from the diameter of the arcs and the associated C for each element was estimated using the relationship $\omega RC=1$ at the arc maxima (where $\omega = 2\pi f$ and f is the frequency (in Hz) at the arc maximum). In all cases, the lower frequency Z* arc had an associated capacitance of ~ 0.1-0.2 nFcm^{-1} for samples sintered at 1200 ℃ and ~ 3-4 nFcm^{-1} for samples sintered at 1450 ℃. Based on the Brick-work Layer Model (BLM) for electroceramics this is consistent with a grain boundary response with the increase in C with sintering temperature being commensurate with an increase in ceramic density. The higher frequency Z* arc had an associated capacitance of ~ 10-20 pFcm^{-1} and decreased systematically with increasing temperature. ST is an incipient ferroelectric with a room temperature relative permittivity, ε_r of ~ 295 which decreases at higher temperature in accordance with the Curie-Weiss law. C values of ~ 10-20 pFcm^{-1} correspond to ε_r values of ~ 100-200 and confirm the high frequency arc to be associated with the bulk (grain) response.

Z* plots for ST ceramics sintered in O_2 at 1200 ℃ and in N_2 at 1450 ℃ are shown in Figs 1 (a) and (b), respectively. IS measurements were initially conducted in the atmosphere employed during the sintering process but was then changed to the other atmosphere to test for the oxygen partial pressure dependence and therefore n- or p-type character of the bulk (R_b) and grain boundary (R_{gb}) regions. For ST sintered at 1200 ℃ in O_2 and measured in a flowing O_2 atmosphere at 400 ℃, the *dc* (total) resistivity, $R_T = R_b + R_{gb}$, obtained from the low frequency intercept on the Z' axis was ~ 2 MΩcm. R_T was dominated by a large grain boundary arc, R_{gb} ~ 1.8 MΩcm, Fig 1 (a) with the bulk component being revealed by a small arc at higher frequencies with R_b ~ 20 kΩcm, inset in Fig 1 (a). Switching the gas atmosphere at 400 ℃ from O_2 to N_2 caused a substantial increase in R values; R_b increased to ~ 120 kΩcm; R_{gb} and R_T exceeded the measuring limit of the instrumentation (~ 10 MΩcm) and therefore it was not possible to observe a complete low frequency grain boundary arc in the Z* plot, Fig 1 (a). For ST sintered at 1450 ℃ in N_2 and measured in a N_2 atmosphere at 500 ℃, R_T ~ 550 kΩcm was again dominated by R_{gb} ~ 520 kΩcm, Fig 1 (b), with R_b being an order of magnitude smaller, ~ 30 kΩcm. Switching the gas atmosphere from N_2 to O_2 at 500 ℃ resulted in a substantial decrease in R_T, R_{gb} and R_b. From the Z* plot in Fig 1 (b); R_T ~ 98 kΩcm; R_{gb} ~ 93 kΩcm and R_b ~ 5kΩcm, inset in Fig 1 (b). For conciseness, Z* plots are not shown for ST ceramics sintered in N_2 at 1200 ℃ or in O_2 at 1450 ℃ but their behaviour was consistent with that described for the two samples above. The bulk conductivity, $\sigma_b = 1/R_b$, is plotted in Arrhenius format for ST ceramics sintered and measured in the same atmosphere in Fig 3 (a). For each temperature, the ceramics sintered in O_2 show slightly higher σ_b; nevertheless all show bulk conduction activation energy (E_a) values of ~ 0.8-1 eV with σ_b ~ 10^{-4} Scm^{-1} at ~ 500 ℃. The increase in σ_b (or a decrease in R_b) with a switch in the measuring pO_2 from an inert (N_2) ambient to flowing oxygen during IS measurements at ~ 400-500 ℃ as shown in Fig. 1 is consistent with p-type conduction in these ceramics.

The IS results obtained from LST ceramics were substantially different to those obtained from ST and were strongly dependent on the sintering temperature. Samples sintered at 1200 ℃ displayed a single arc in the Z* plots, irrespective of the atmosphere used in the sintering process and could be modeled on a single RC

element. The associated C of the arc shown for LST sintered at 1200 ℃ in O_2 and measured at 650 ℃ in flowing oxygen was ~ 12.2 pFcm^{-1} and therefore consistent with a bulk response. R_b in the O_2 ambient at 650 ℃ was ~ 130 kΩcm but decreased to ~ 6 kΩcm on switching to N_2, inset Fig 2 (a). LST samples sintered at 1200 ℃ in N_2 displayed similar Z* plots and pO_2 behaviour of R_b indicating n-type conduction, as opposed to the p-type observed for ST. Arrhenius plots of σ_b for LST ceramics sintered at 1200 ℃ and measured in the same gas flowing atmosphere reveal σ_b to be less conductive than ST ceramics with a much higher E_a of ~ 1.6-1.8 eV, Fig 3 (b).

The IS results for LST ceramics sintered at 1450 ℃ showed them to be electrically heterogeneous with the presence of a resistive surface layer that could be removed on polishing the ceramics. Typical Z* plots at room temperature (RT) are shown in Figs 2 (b) and (d) for samples sintered in flowing O_2 and N_2, respectively. Before polishing, the *dc* (total) resistivity of the O_2 fired ceramics exceeded > 10 MΩcm but decreased to ~ 80 kΩcm on reducing the pellet thickness by ~ 58 % from 5.36 to 2.25 mm, Fig 2 (b). A reduction in pellet thickness of ~ 46 % from 6.05 to 3.27 mm reduced the total resistivity of the N_2 fired ceramic from ~ 546 Ωcm, Fig 2 (d) to ~ 2.4 Ωcm, inset in Fig 2 (d). The Z* response at RT of an LST ceramic sintered in O_2 after polishing consisted of three over-lapping poorly resolved arcs. Subambient measurements in the range ~ 110-210 K were able to resolve a high frequency arc with an associated C ~ 40-60 pFcm^{-1} that was consistent with a high ε_r bulk response, see Fig 2 (c). An Arrhenius plot of σ_b for LST sintered in O_2 at 1450 ℃ shows the grains to be semiconducting below RT with E_a ~ 0.16 eV. To confirm the Z* arc in Fig 2 (c) was associated with a bulk response, IS data were plotted in the form of imaginary component of electric modulus, M", spectroscopic plots (Fig S2) as M" plots are known to be sensitive to bulk responses.[29] The frequency of the Z" peak maximum (f_{max}) associated with the arc in the Z* plot of Fig 2 (c) was similar to that of a large M" Debye peak with an associated capacitance of ~ 50 pFcm^{-1} confirming the assignment of this response to a bulk component. f_{max} associated with this M" Debye peak could be obtained over the temperature range ~ 110-210 K with $M"_{max}$ of the peak increasing with temperature, Fig S2, indicating C_b and therefore, ε_r to decrease with increasing temperature as expected for ST-based materials.

The LST ceramics sintered in N_2 at 1450 ℃ were more conductive with a less resistive surface layer when compared to those sintered in O_2 at the same temperature. Subambient measurements were conducted on an ceramic after removal of the resistive surface layer (not shown). It was not possible to observe a bulk response in either Z* or Z", M" spectroscopic plots down to 10 K and therefore σ_b was too conductive (> 0.1 Scm^{-1}) to measure by IS. Two components were resolved in the range 70-170 K, Fig S3(a). A semiconducting component in the Z" spectra with a temperature independent C of ~ 0.1 μFcm^{-1} and R in the range 10^2-10^5 Ωcm with E_a ~ 0.05 eV and another semiconducting component associated with a small M" peak with a temperature independent C of ~ 10 $nFcm^{-1}$ and R in the range 10^2-10^4 Ωcm also with E_a ~ 0.06 eV, Fig S3(b)-(d). Although full identification of these components is outside the scope of this script, the most likely explanation is the Z" component is associated with a non-ohmic contact to the semiconducting ceramic with the small M" component being associated with a residual surface layer/grain boundary component.

Discussion.

The results obtained for ST ceramics are consistent with the acceptor-doped model for $(Ba,Sr,Ca)TiO_3$ perovskites.[11,30] Low levels of oxygen vacancies exist in undoped $(Ba,Sr,Ca)TiO_3$ perovskites, presumably due to the presence of aliovalent impurities such as Fe^{3+} and Al^{3+} in TiO_2 reagents. Oxygen up-take can occur to fill the oxygen vacancies and create p-type holes based on the following reaction

$$V_O^{\bullet\bullet} + ½\ O_2\ (g) \rightarrow O_O^{x} + 2\ h^{\bullet} \quad \text{(equation 2)}$$

E_a associated with this extrinsic conduction mechanism is commonly reported to be ~ 0.8 to 1 eV and our ST sintered ceramics, Fig 3 (a) are in agreement with these values. The similar levels of σ_b for ST ceramics sintered in O_2 and N_2 at 1200 and 1450 ℃ indicate all samples have similar oxygen contents and that significant net oxygen-loss does not occur from undoped ST ceramics sintered at 1450 ℃ in an inert atmosphere such as flowing N_2.

The LST ceramics are single phase by XRD, confirming the A-site vacancy doping mechanism of $3\ Sr_{Sr}^{x} \rightarrow 2\ La_{Sr}^{/} + V_{Sr}^{\bullet\bullet}$ reported by other workers[6-9,23] to occur at least to a dopant level of 10 % La on the A-site. The creation of A-site vacancies that

are immobile below ~ 1000 ℃ should not influence σ_b; however, IS results for LST samples are noticeably different to that for ST sintered under similar conditions, Fig 2. For samples sintered at 1200 ℃; (i) σ_b below 500 ℃ is at least three orders of magnitude lower for LST compared to ST, irrespective of atmosphere; (ii) E_a associated with bulk conduction increases from ~ 0.8-1.0 eV for ST to 1.6 eV for LST; (iii) there is a switch from p-type to n-type behaviour with La-doping. Increasing the sintering temperature for LST to 1450 ℃ results in electrically heterogeneous ceramics, irrespective of the sintering atmosphere.

Combining (i) to (iii) suggests the p-type hole concentration that exists in ST has been annihilated by n-type electron carriers, i.e. $e^{/} + h^{\bullet}$ = nil, by the loss of a small amount of lattice oxygen based on equation 1. LST sintered at 1200 ℃ in either O_2 or N_2 are homogeneous dielectrics, Fig 2 (a), with $\sigma_b \sim 10^{-7}$ Scm^{-1} at ~ 500 ℃ with an E_a of ~ 1.6 eV, Fig 3 (b), which is consistent with near intrinsic conduction across the Band gap (E_g) for $SrTiO_3$, given E_g ~ 3.2 eV for $SrTiO_3$ and $E_a \sim E_g/2$ for intrinsic band-type conduction.[30] The level of oxygen loss (δ) from LST ceramics increases rapidly for the higher sintering temperature of 1450 ℃ resulting in significant n-type grain semiconductivity, based on the magnitude of σ_b and low Ea < 0.2 eV for O_2 fired ceramics at subambient temperatures and the inability of IS to quantify σ_b for samples sintered in N_2. The increase in electron concentration associated with the increased loss of lattice oxygen results in partial reduction of Ti^{4+} to Ti^{3+} ions which facilitates conduction in the Ti 3d conduction band. The resistive surface layers and heterogeneous electrical microstructures observed by IS for LST ceramics sintered at 1450 ℃, Fig 2 (b)-(d), are a result of limited re-oxidation on cooling and are similar to those reported for La-doped $BaTiO_3$ ceramics.[19] Such electrical microstructures are strong evidence for the occurrence of oxygen-loss in A-site deficient LST ceramics. It is noteworthy that the oxygen-loss process starts to occur in LST at temperatures as low as 1200 ℃ even when processing in a flowing O_2 gas environment. This is in contrast to B-site deficient $Ba_{1-x}La_xTi_{1-x/4}O_3$ ceramics where significant oxygen-loss can be suppressed at a sintering temperature of 1350 ℃ for all x by processing in flowing O_2.[15,19,20]

It is clear that A- and B-site vacancies play a dramatic role in the ability to lose lattice oxygen in titanate-based perovskites and this can be used to modify the electrical

properties La-doped (Ba,Sr)TiO_3 materials. Atomistic simulations are in progress to detail the influence of A-site vacancies on the ease with which oxygen can be liberated from La-doped ST to create n-type conductivity. Strongly reduced ST-based ceramics are potentially useful for applications based on anodes for SOFC's and internal barrier layer capacitors but this behaviour needs to be avoided or suppressed for homogeneous bulk dielectric materials.

Acknowledgements.

IA thanks the Scientific and Technological Research Council of Turkey (TUBITAK) for financial support via the 2219-International Postdoctoral Research Fellowship Programme.

References

[1] H. Kishi, Y. Mizuno, and H. Chazono, *Jpn. J. Appl. Phys.*, 2003, **42**, 1.

[2] D. Neagu and J. T. S. Irvine, *Chem. Mater*., 2011, **23**, 1607.

[3] H. Suzuki, H. Bando, Y. Ootuka, I.H. Inoue, T. Yamamoto, K. Takahashi and Y. Nishihara, *J. Phys. Soc. Jpn.,* 1996, **65**, 1529.

[4] A. Ohtomo and H. Y. Hwang, *Nature (London)* 2004, **427**, 423.

[5] D. Neagu and J. T. S. Irvine, *Chem. Mater*., 2010, **22**, 5042.

[6] G. H. Jonker, *Solid-State Electron*., 1964, **7**, 895.

[7] T. Y. Tien and F. A. Hummel, *Trans. Br. Ceram. Soc*., 1967, **66**, 233.

[8] J. Bouwma, K. J. DeVries and A. J. Burggraaf, *Phys. Status Solidi*, 1976, **A35**, 281.

[9] S. Shirasaki, M. Tsukioka, H. Yamamura, H. Oshima and K. Kakegawa, *Solid State Commun*., 1976, **19**, 721.

[10] U. Balachandran and N. G. Eror, *Commun. Am. Ceram. Soc.*, 1981, **64**, C75.

[11] G. H. Jonker and E. E. Havinga, *Mater. Res. Bull*., 1982, **17**, 345.

[12] B. F. Flandermeyer, A .K. Agarwal, H. U. Anderson and M. M. Nasrallah, *J. Mater. Sci., 1984,* **19**, 2593..

[13] R. Moos, T. Bischoff, W. Menesklou and K. H. Hardtl, *J. Mater. Sci., 1997*, **32**, 4247.

[14] D. M. Smyth, *The Defect Chemistry of Metal Oxides*, Oxford University Press, 2000.

[15] F. D. Morrison, A. M. Coats, D. C. Sinclair and A. R. West, *J. Electroceram.*, 2001, **6**, 219.

[16] D. Makovec, Z. Samardzija, U. Delalut and D. Kolar, *J. Am. Ceram. Soc.*, 1995, **78**, 2193.

[17] F. D. Morrison, D. C. Sinclair and A. R. West, *J. Am. Ceram. Soc*., 2001, **84**, 474.

[18] G. V. Lewis and C. R. A. Catlow, *J. Phys. Chem. Solids*, 1986, **47**, 89.

[19] F. D. Morrison, D. C. Sinclair and A. R. West, *J. Am. Ceram. Soc.*, 2001, **84**, 531.

[20] F. D. Morrison, D. C. Sinclair and A. R. West, *J. Appl. Phys*., 1999, **86**, 6355.

[21] C. L. Freeman, J. A. Dawson, H. R. Chen, J. H. Harding, L. Ben and D. C. Sinclair, *J. Mater. Chem*., 2011, **21**, 4861.

[22] C. L. Freeman, J .A. Dawson, H. R. Chen, L. Ben, J. H. Harding, F. D. Morrison, D. C. Sinclair and A. R. West, *Adv. Funct. Mater.*, 2013, **23**, 3925.

[23] C. H. Howard, G. R. Lumpkin, R. I. Smith and Z. Zhang, *J. Solid State Chem.*, 2004, **177**, 2726.

[24] J. A. Dawson, X. Li, C. L. Freeman, J. H. Harding and D. C. Sinclair, *J. Mater. Chem.*, 2013, **C1**, 1574.

[25] S. Hui and A. Petric, *J. Electrochem. Soc.*, 2002, **149**, J1.

[26] C. D. Savaniu, D. N. Miller and J. T. S. Irvine, *J. Am. Ceram. Soc.*, 2013, **96**, 1718.

[27] P. R. Slater, D .P. Fagg and J. T. S. Irvine, *J. Mater. Chem.*, 1997, **7**, 2495.

[28] O. A. Marina and L. R. Pederson, Proceedings of the 5th European Solid Oxide Fuel Cell Forum, Edited by J. Huijsmans, Lucerne, Switzerland, 2002.

[29] D. C. Sinclair and A. R. West, *J. Appl. Phys.*, 1989, **66,** 3850.

[30] R. Moos and K. H. Hardtl, *J. Am. Ceram. Soc.*, 1997, **80**, 2549.

Table 1. Lattice parameter, cell volume, relative density, bulk conductivity and activation energy, E_a for all samples.

Sample	*a* (Å)	V (Å^3)	Relative density (%)	Bulk conductivity at 500 ^{o}C (S cm^{-1})	Bulk E_a (eV)
ST 1200 ℃ O_2	3.90540(6)	59.566(2)	69.5	2.0×10^{-4}	0.82 (0.09)
ST 1200 ℃ N_2	3.90543(3)	59.567(1)	65.1	7.1×10^{-5}	1.04 (0.04)
ST 1450 ℃ O_2	3.90557(19)	59.574(5)	98.4	5.2×10^{-5}	0.97 (0.03)
ST 1450 ℃ N_2	3.90551(20)	59.571(5)	97.2	3.4×10^{-5}	1.02 (0.02)
LST 1200 ℃ O_2	3.90104(9)	59.367(2)	61.5	1.8×10^{-7}	1.64 (0.02)
LST 1200 ℃ N_2	3.90212(7)	59.416(2)	61.0	3.6×10^{-7}	1.79 (0.02)
LST 1450 ℃ O_2	3.90233(12)	59.425(3)	99.3	Too conductive to be measured at 500 ℃. 1.0×10^{-4} at 210 K	0.16 (0.01)
LST 1450 ℃ N_2	3.90220(4)	59.419(1)	98.4	Too conductive ($> 10^{-1}$) to be measured at 10 K	

Figure Captions

Figure 1: Z^* plots of $SrTiO_3$ ceramics, (a) sintered at 1200 ℃ in O_2 and measured at 400 ℃ in O_2 and N_2 and (b) sintered at 1450 ℃ in N_2 and measured at 500 ℃ in N_2 and O_2. Insets show an enlargement of high frequency data. Selected frequency values are labelled.

Figure 2: Z^* plots of $Sr_{0.85}La_{0.10}TiO_3$ ceramics, (a) sintered at 1200 ℃ in O_2 and measured at 650 ℃ in O_2 and N_2, (b) sintered at 1450 ℃ in O_2 and measured at room temperature (RT) in air before and after polishing, (c) sintered at 1450 ℃ in O_2 and measured at 150 K in vacuum, (d) sintered at 1450 ℃ in N_2 and measured at RT in air before and after polishing. Insets show an enlargement of high frequency data. Selected frequency values are labelled.

Figure 3: Arrhenius plots comparing σ_b of (a) $SrTiO_3$ and (b) $Sr_{0.85}La_{0.10}TiO_3$ ceramics sintered at 1200 ℃ and 1450 ℃ for 6 h, in O_2 and N_2 atmospheres. For each sample, the conductivity was obtained by measuring in the same atmosphere as used for sintering.

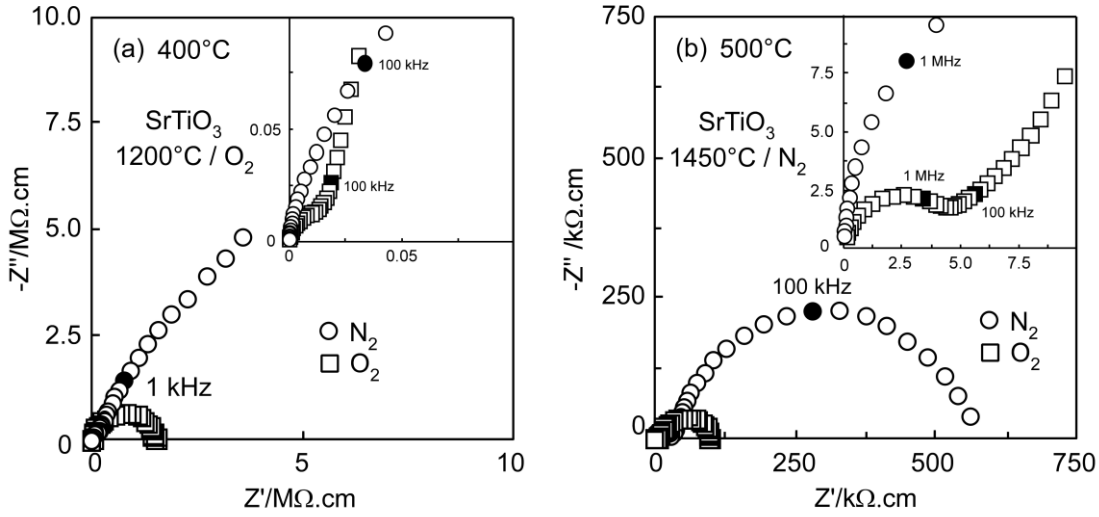

Figure 1

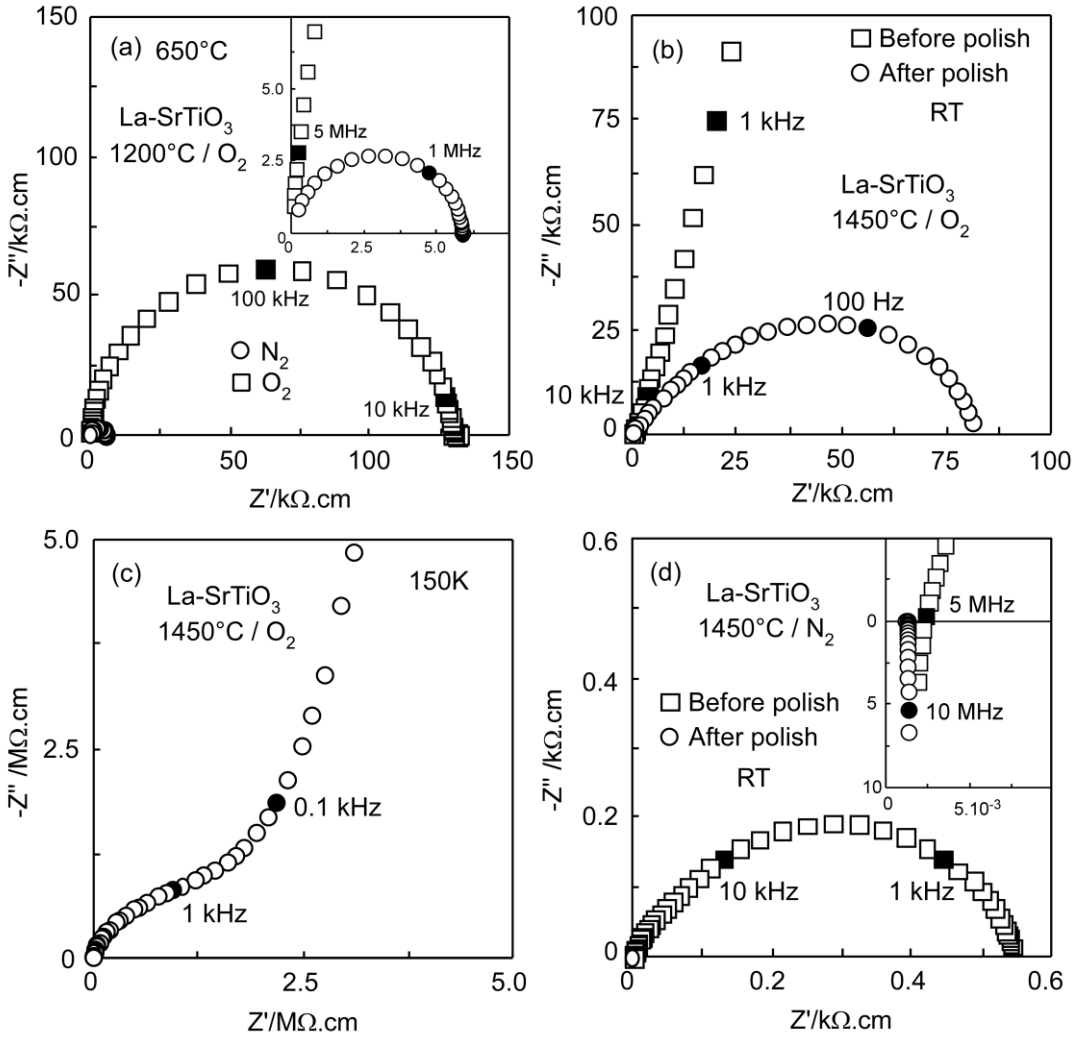

Figure 2

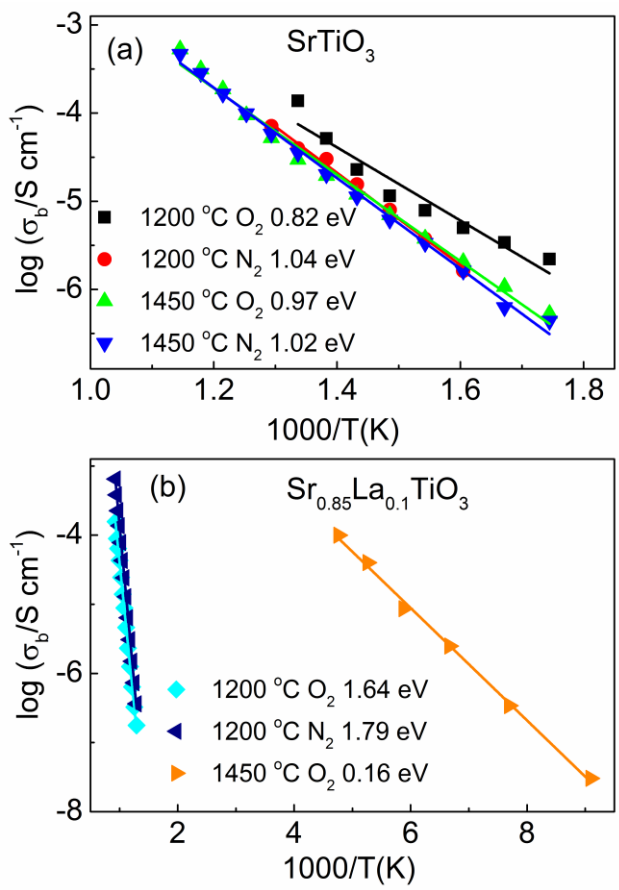

Figure 3